View metadata, citation and similar papers at core.ac.uk

brought to you by CORE

provided by Elsevier - Publisher Connector

Neoplasia • Vol. 9, No. 5, May 2007, pp. 392–400 392

www.neoplasia.com

Early Changes in Apparent Diffusion Coefficient Predict the Quantitative Antitumoral Activity of Capecitabine, Oxaliplatin, and Irradiation in HT29 Xenografts in Athymic Nude Mice[1]

Therese Seierstad[*,†,¶], *Sigurd Folkvord*[‡], *Kathrine Røe*[†], *Kjersti Flatmark*[‡], *Arne Skretting*[*] *and Dag Rune Olsen*[†,§]

Departments of *Medical Physics, [†]Radiation Biology, and [‡]Tumor Biology, Rikshospitalet-Radiumhospitalet Medical Center, Oslo, Norway; [§]University of Oslo, Oslo, Norway; [¶]Buskerud University College, Faculty of Health, Drammen, Norway

Abstract

PURPOSE: **The purpose of this study was to evaluate the possible use of changes in apparent diffusion coefficient (ADC) measured by magnetic resonance imaging for pretreatment prediction and early detection of tumor response in a mouse model during fractionated chemoradiotherapy.** ***MATERIALS AND METHODS:*** **Athymic mice with bilateral HT29 xenografts on rear flanks were allocated into three groups: control, capecitabine, and capecitabine and oxaliplatin. The left flanks of the mice received daily irradiation.** T_2 **and diffusion images were acquired before therapy and weekly for the following 9 weeks. Pretreatment and changes in ADC were calculated and compared with tumor doubling growth delay.** ***RESULTS:*** **No correlations between pretreatment ADC and changes in tumor volumes after therapy were seen. All treated tumors, except those receiving capecitabine (*P* = .06), showed increased mean tumor ADC values 11 days after initialization of therapy (*P* < .05) before returning to pretreatment values within 5 days posttherapy (day 18 after onset of therapy). This increase in mean tumor ADC showed a strong positive correlation (*r* = 0.92, *P* < .01) with mean tumor doubling growth delay.** ***CONCLUSIONS:*** **Pretreatment ADC values did not predict the effectiveness of therapy, whereas early changes in mean ADC quantitatively correlated with treatment outcome.**

Neoplasia (2007) **9,** 392–400

Keywords: Apparent diffusion coefficient, HT29, oxaliplatin, capecitabine, prediction of therapy response.

Introduction

Colorectal cancer is estimated to be the second leading cause of cancer deaths worldwide [1]. Approximately 35% of colorectal cancers are located in the rectum, and prognosis depends on the tumor's degree of penetration through the bowel wall, lymph node involvement, and existence of distant metastasis. Treatment advances, such as the standardized surgical technique of total mesorectal excision [2] and preoperative radiotherapy with or without concomitant systemic chemotherapy, have decreased the previously high local recurrence rate and have improved survival in rectal cancer patients [3–6]. Despite these advances, about 40% of patients die from disseminated disease. Early markers of therapy response have the potential to enable oncologists to adjust therapeutic intervention during the course of treatment, giving a potential for improved survival for these patients.

Diffusion-weighted magnetic resonance imaging (DW-MRI) provides information about the tissue microenvironment and is able to detect molecular and cellular changes preceding macroscopic changes in tumor size, regression, and growth [7–13]. The diffusion of water in tissue may be assessed by apparent diffusion coefficient (ADC) measured by DW-MRI. In DW-MRI, MR signal is made dependent on water mobility by incorporating a set of additional bipolar pulsed magnetic field gradients into the MR sequence [14]. Individual water protons (spins) will accumulate a phase shift proportional to their position in the gradient field. After waiting for an evolution time for water protons to diffuse, an inverse refocusing gradient is applied. Stationary water protons are completely refocused, whereas the refocusing of mobile water protons is incomplete. Signal intensity in diffusion-weighted images depends on b value. For the commonly used pulsed gradient spin-echo diffusion sensitization scheme, the b value is given by $b = \gamma^2\delta^2G^2(\Delta - \delta/3)$, where γ is the gyromagnetic ratio, G is the magnitude of diffusion-encoding gradients, δ is the duration of each diffusion-encoding gradient, and Δ is the time interval between diffusion-encoding gradients. Thus, the MR signal is made proportional to local tissue water mobility. The diffusion of water in tissue is strongly affected by molecular viscosity and membrane permeability between intracellular and extracellular

Address all correspondence to: Therese Seierstad, Department of Medical Physics, Rikshospitalet-Radiumhospitalet Medical Center, Montebello, Oslo 0310, Norway.
E-mail: therese@radium.uio.no

[1]This study was supported by grant no. D 04085/003 from the Norwegian Cancer Society.
Received 31 January 2007; Revised 29 March 2007; Accepted 2 April 2007.

Copyright © 2007 Neoplasia Press, Inc. All rights reserved 1522-8002/07/$25.00
DOI 10.1593/neo.07154

compartments, active transport and flow, and directionality of structures that impede or enhance water mobility [8,9]. Recent work has demonstrated that the ADC value of a tissue is strongly dependent on microscopic changes in tissue structure and physiology [15], and several groups have shown increased water diffusion in experimental tumors as a response to successful therapies [7–13]. This increase is most likely due to a shift of water from the intracellular space to the extracellular space [8,9]. As cells are killed by therapeutic interventions, the integrity of cell membranes may be compromised, and the fractional volume of interstitial space is increased due to apoptosis-induced cell shrinkage and necrosis. Damage to tissue microvasculature may also lead to vasogenic edema, thereby reducing the viscosity of interstitial fluid and increasing extracellular volume. A reduced cell volume fraction will result in an overall increase in ADC because water molecules in the extracellular space move more freely than water protons in the intracellular space [9].

More than 40 years after its development, 5-fluorouracil (5-FU) remains the most used chemotherapeutic agent for the treatment of many types of cancer; for locally advanced rectal cancer, 5-FU is the standard radiosensitizing agent [16]. Data from phase I/II single-agent and combination capecitabine chemoradiation studies provide a clear rationale for replacing infusional 5-FU with the orally administered 5-FU prodrug capecitabine as part of chemoradiation for patients with locally advanced rectal cancer [17]. The availability of new radiosensitizing drugs that may be combined with 5-FU offers an opportunity to improve the effectiveness of therapy, and there are several clinical studies evaluating the effect of integrating oxaliplatin into the treatment regime for locally advanced rectal cancer [18–24]. Capecitabine and oxaliplatin both possess radiosensitizing properties [25–28], and several phase I and phase II studies indicate that preoperative capecitabine/oxaliplatin chemoradiation is effective and generally well tolerated [29–32].

Traditionally, the first indications of the effectiveness of a therapeutic intervention have been changes in tumor volume and other clinical observable factors. These changes occur late in the course of therapy, and the predictive power of conventional response is, however, limited. Recent studies suggest that the ADC of water, which is measured noninvasively with MRI, is a sensitive and reliable way of monitoring response to therapeutic interventions. To our knowledge, there have been no experimental studies addressing the predictive value of early changes in ADC using irradiation and chemotherapy. The purpose of this study is, thus, to investigate whether ADC measurements can be used in response prediction and early monitoring following concomitant chemoradiotherapy.

Materials and Methods

Chemicals

Capecitabine (Xeloda; Roche, Hertfordshire, UK) powder was suspended in vehicle [40 mM citrate buffer containing 5% (wt/vol) gum arabic, pH 6.0]. Liquid oxaliplatin (Eloxatin; 5 mg/ml) was purchased from Sanofi Synthelabo (Gentilly, France). A stock solution of oxaliplatin was diluted five times in 5% glucose solution for intravenous injection, as recommended by the supplier.

Animals and Xenografts

Thirty-five female BALB/c nude mice (nu^+/nu^+) weighing 20 to 30 g and aged 6 to 8 weeks old were used in this study. The National Committee on Research on Animal Care approved the animal protocol, and the experiment was performed according to Interdisciplinary Principles and Guidelines for the Use of Animals in Research, Marketing, and Education (New York Academy of Science, New York, NY). The mice were bred at the animal department of our institute and kept under specific pathogen-free conditions at constant temperature (22–24°C) and humidity (30–50%). The mice were given sterilized food and tap water *ad libitum*. Tumor tissue fragments of the human colon adenocarcinoma HT29 cell line, each measuring $\sim 2 \times 2 \times 2$ $(mm)^3$, were transplanted subcutaneously and bilaterally into the rear flanks of mice to generate HT29 xenografts. Treatment began 5 weeks after inoculation, with mice bearing 100-mm^3 to 340-mm^3 subcutaneous tumors.

Assessment of Therapy Response

In axial T_2-weighted fast spin-echo MR images, the tumors appeared with high signal intensity relative to that of the neighboring muscle (Figure 1). Manually circumscribed regions of interest delineating the tumor volume in each slice were multiplied by slice thickness to obtain tumor volumes. Tumors were observed until the volume of one of the two bilateral tumors on the rear flanks of the mice had reached four times its pretreatment volume. The effectiveness of therapy was evaluated by tumor doubling growth delay (Td) and was calculated according to the following formula: Tumor Doubling Growth Delay (Td) = $T_{2x} - C_{2x}$, where T_{2x} and C_{2x}

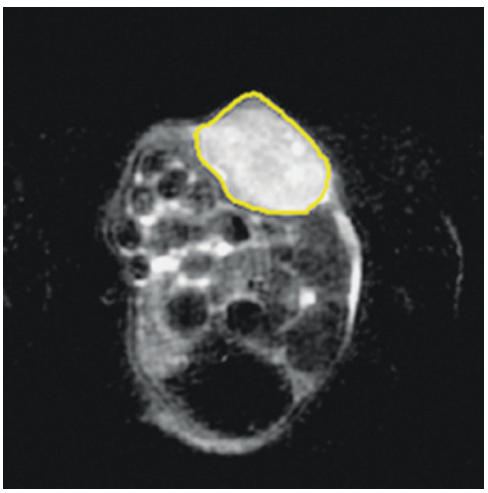

Figure 1. *Axial T_2-weighted MR image obtained with a fast spin-echo sequence of a mouse showing the HT29 tumor appearing bright relative to surrounding tissues, allowing easy delineation of tumor borders.*

represent the number of days that treated and control tumors take to double in size from the first day of treatment, respectively. The expected Td in days of combined treatment was calculated according to the following formula [33]: Expected $Td_{modality1+modality2} = Td_{modality1} + Td_{modality2}$, with the modalities being capecitabine, oxaliplatin, and irradiation. The effect of the combined treatment (synergistic/additive/antagonistic) was assessed by calculating the ratio of observed Td divided by that of expected Td. The observed/expected ratios were as follows: > 1 (combination was synergistic), < 1 (combination was antagonistic), and 1 (combination was additive) [33].

Treatment

The tumors were pooled and randomly allocated into three groups: control (group 1), capecitabine (group 2), and capecitabine and oxaliplatin (group 3). Capecitabine (359 mg/kg per day) or vehicle was administered by oral gavage 5 days/week for 2 weeks (days 1–5 and 8–12). The animals in group 3 received oxaliplatin (10 mg/kg) as an intravenous injection on days 2 and 9, whereas the mice in groups 1 and 2 were given intravenous injections of 5% glucose solutions. Fractionated irradiation (2 Gy × 10 on days 2–6 and 9–13) was delivered using a ^{60}Co unit (Mobaltron 80; TEM Instruments, Crawley, UK) at a dose rate of 0.6 Gy/min. The megavolt beam produced by this cobalt source gives an initial dose buildup with depth, resulting in a maximum dose at a depth of 4 mm. To achieve a homogeneous dose deposition within the tumor volume, a 5-mm-thick polystyrene bolus was placed on top of the tumor. During radiotherapy, the left flanks of anesthetized mice were irradiated, whereas the rest of the body (including the contralateral tumor) was kept outside the radiation field. Irradiation was performed 30 minutes after chemotherapy administration.

The mice were anesthetized with subcutaneous injections of a mixture of 2.4 mg/ml tiletamine and 2.4 mg/ml zolazepam (Zoletil vet; Virbac Laboratories, Carros, France), 3.8 mg/ml xylazine (Narcoxyl vet; Roche, Basel, Switzerland), and 0.1 mg/ml butorphanol (Torbugesic; Fort Dodge Laboratories, Fort Dodge, IA), given as a dose of 25 mg/kg before chemotherapy and/or irradiation and 75 mg/kg before MR examinations.

MRI

All experiments were performed on a 1.5-T GE Signa LS clinical whole-body scanner (GE Medical Systems, Milwaukee, WI) equipped with a conventional gradient system (30 mT/m). The anesthetized mouse was placed in a special cradle and put into an in-house–built high-resolution dedicated mouse MR coil (Figure 2). The loaded MR coil was manually fine-tuned to the resonance frequency of the MR scanner before the coil was placed inside the bore of the magnet. All MR exams consisted of axial fast spin-echo T_2-weighted high-resolution images ($T_{E\ eff}$ = 85 milliseconds; T_R = 4000 milliseconds; echo train length (ETL) = 16; slice thickness = 2 mm; image matrix = 192 × 160; field of view = 4 cm), diffusion tensor images (diffusion-weighted single-shot fast spin echo $T_{E\ eff}$ = 78.7 milliseconds; T_R = 5000 milliseconds; field of view = 14 cm; image matrix = 128 × 128; slice thickness = 2 mm; interslice gap = 1 mm; b = 0 and 300 sec/mm^2; with the following x, y, and z gradient directions [1 0 1], [−1 0 1], [0 1 1], [0 1 −1], [1 1 0], [−1 1 0]), and axial fast spin-echo T_2-weighted images with identical fields of view as diffusion images. Preliminary diffusion tensor imaging of the HT29 tumor model showed no appreciable diffusion anisotropy at this spatial resolution, and it was reasonably assumed that diffusion in this HT29 tumor model is isotropic (data not published). Nonetheless, six diffusion gradient directions were used to acquire data. By using the commercially available nICE software (Nordic Neurolab, Bergen, Norway), acquired data were averaged on a pixel-by-pixel basis to obtain isotropic ADCs. The mean ADC values of the tumors were found by manually delineating the tumor tissue in T_2-weighted images and copying these regions of interest to corresponding ADC maps. The change in ADC values following therapy was determined by calculating the percent change in mean water ADC from baseline, with each mouse serving as its own control. %ADC4, %ADC11, . . ., %ADC60 corresponds to the percent change in mean tumor ADC from before therapy to day 4, day 11, . . ., day 60 after onset of therapy, respectively.

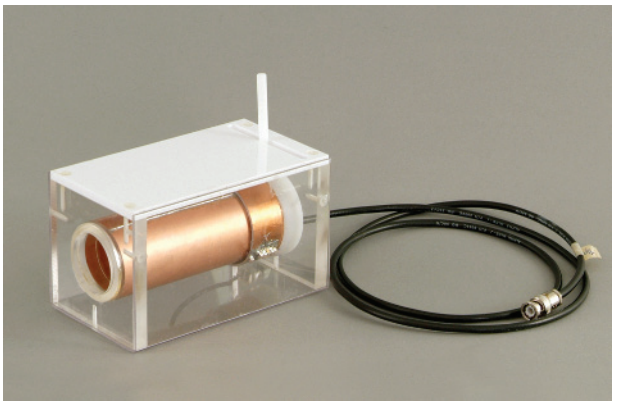

Figure 2. *In-house–built capacitive overlap transmit–receive MR mouse coil for the imaging of small animals with a clinical whole-body scanner.*

Histologic Sections

After the last MR examination, the mice were sacrificed by cervical dislocation, and the orientation of the tumors in the magnet was marked on the surrounding tumor skin. The tumors were immediately excised and fixed in 4% formalin overnight. The tumors were imbedded in paraffin, and a 5-μm-thick section corresponding to the MR slice was stained with hematoxylin and eosin (HE). Necrotic fraction was found in all HE stains.

Statistical Analysis

Statistical analysis was performed using SPSS 13.0 (SPSS, Cary, NC). The Kolmogorov-Smirnov test was applied to test for normality of tumor volumes and ADC values. Two of the tumors in the experiment did not double their volumes during the 60 days that the experiment lasted, and their tumor doubling times were set to the maximum

observation period. Differences in tumor doubling growth delays between treatment groups were compared using one-way analysis of variance (ANOVA) and *t*-test. Pearson's correlation test was used to analyze whether the correlation between two variables was significant. A significance level of 5% was used in all statistical analyses.

Results

Tumor Growth Curves

Statistical normality analysis with the Kolmogorov-Smirnov test revealed that tumor volumes were normally distributed before the onset of therapy (P = .34). The response of HT29 xenografts to irradiation alone and in combination with capecitabine and oxaliplatin is shown in Figure 3. Untreated exponentially growing xenografts (n = 8) had a doubling time of 18.1 ± 1.7 days. For all HT29 xenografts receiving radiotherapy or chemoradiation, a significant antitumor activity was observed (P < .05). As monotherapy, radiation (n = 9) was most effective, with a tumor doubling growth delay of 13.9 ± 4.0 days, followed by capecitabine (Td = 7.0 ± 2.3 days; n = 13). Furthermore, the antitumor activity of the capecitabine/oxaliplatin combination treatment (Td = 14.1 ± 1.7 days; n = 10) was significantly greater than that of capecitabine (n = 13) alone (P = .03). Radiotherapy induced a significant antitumor effect in all HT29 xenografts compared to their contralateral nonirradiated xenografts (P < .01 in all three groups). The eight tumors receiving both daily capecitabine and irradiation for 2 weeks showed a tumor doubling growth delay of 26.5 ± 5.7 days. The most substantial antitumor effect was observed for the combination of capecitabine, oxaliplatin, and irradiation (n = 9), which resulted in initial regression followed by slow regrowth, yielding a tumor growth doubling delay of 30.1 ± 3.3 days. However, the difference in tumor doubling growth delay between the capecitabine/irradiation and capecitabine/oxaliplatin/irradiation groups is not statistically significant (P = .22).

In HT29 xenografts, the observed/expected Td ratio for capecitabine and irradiation was 1.27, indicating that the *in vivo* combination of these two modalities resulted in a synergistic antitumor activity. The *in vivo* combination of capecitabine/oxaliplatin and irradiation had an observed/expected Td ratio of 1.07, indicating at least an additive effect in HT29 xenografts.

ADCs

DW-MRI was used for monitoring the response of HT29 tumor xenografts to combined treatments of capecitabine, oxaliplatin, and irradiation. Statistical analysis revealed a normal distribution of pretreatment ADC values (Kolmogorov-Smirnov, P = .66), with a mean ADC value of 0.53 × 10^{-3} mm^2/sec (range, 0.45 × 10^{-3} to 0.63 × 10^{-3} mm^2/sec; n = 57). ADC maps and high-resolution axial T_2-weighted images from one of the treated animals before therapy, during therapy, and at different times posttherapy are shown in Figure 4. Changes in mean tumor ADC for nonirradiated and irradiated tumors as a result of therapy are presented in Figure 5, *A* and *B*. Pretreatment ADC values were not significantly different between mice in the control group and mice in the treated groups. For control tumors, there were no statistically significant changes in mean tumor ADC during the 9 weeks that the mice were monitored (P > .05 for all time intervals). For all tumors, except those receiving capecitabine (P = .06), the increase in mean tumor ADC from baseline to day 11 was statistically significant (P < .05). On day 18 (5 days after the therapy ended), ADC values had returned to pretreatment levels.

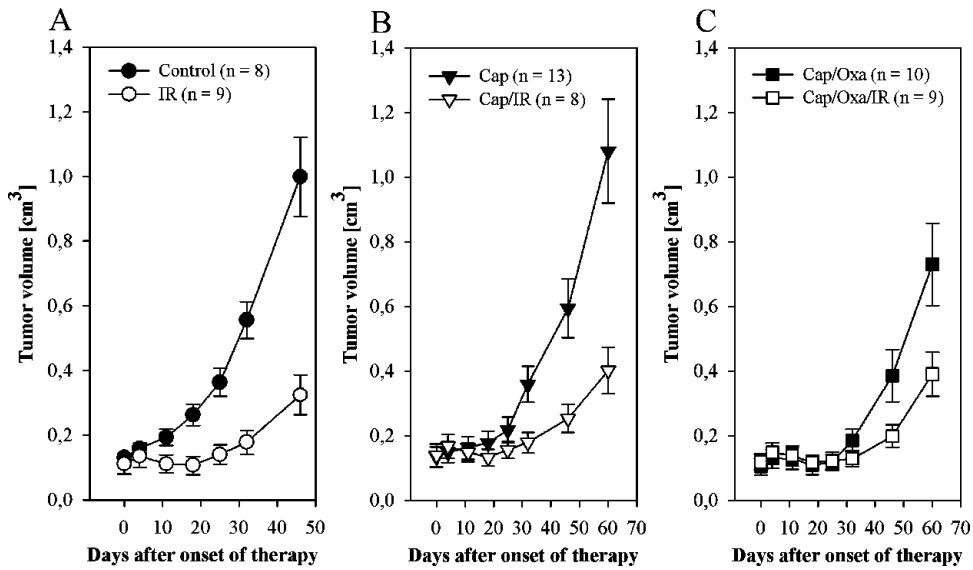

Figure 3. In vivo *efficacy of combined irradiation (2 Gy for five consecutive days, 5 days/week for 2 weeks starting on day 2), capecitabine (359 mg/kg per day, 5 days/week for 2 weeks starting on day 1), and oxaliplatin (10 mg/kg, days 2 and 9) against human colon cancer HT29 xenografts in nude mice: (A) control, (B) capecitabine, and (C) capecitabine and oxaliplatin. All left-sided tumors received additional radiotherapy.*

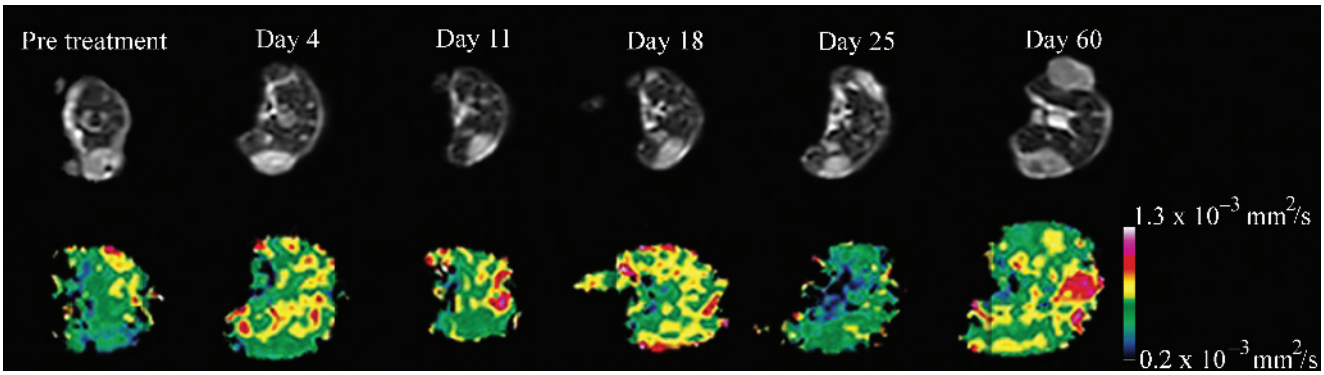

Figure 4. *T_2-weighted MR images (top) and ADC maps (bottom) obtained before therapy, during therapy, and at different times posttherapy from one of the mice that received combined oxaliplatin/capecitabine chemoradiation.*

Pairwise comparisons of %ADC11 for the five treatment groups showed statistically significant differences between capecitabine and capecitabine/oxaliplatin ($P < .01$) and between capecitabine and capecitabine/irradiation ($P < .01$). The differences in %ADC11 between capecitabine/irradiation and capecitabine/oxaliplatin/irradiation and between capecitabine/oxaliplatin and capecitabine/oxaliplatin/irradiation were not statistically significant.

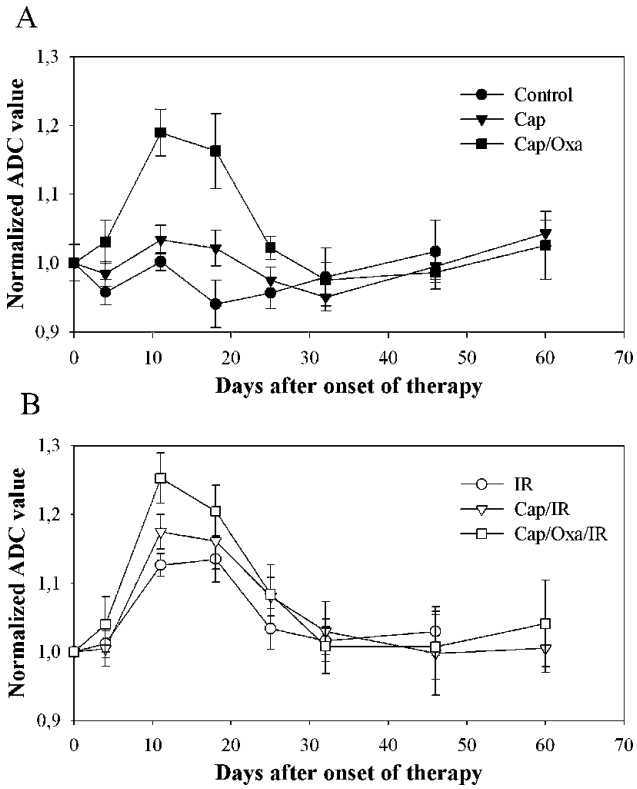

Figure 5. *Changes in mean tumor ADC for nonirradiated (A) and irradiated tumors (B) as a function of time. The ADC value of each tumor is normalized with respect to the pretreatment ADC value. Chemoradiotherapy was given from days 1 to 13, and consisted of oxaliplatin (10 mg/kg, days 2 and 9), capecitabine (359 mg/kg per day, 5 days/week for 2 weeks starting on day 1), and irradiation (2 Gy for five consecutive days, 5 days/week for 2 weeks starting on day 2).*

There were no obvious correlations between the mean tumor ADC before treatment and the observed tumor growth delay for the five treated groups (Figure 6), with Pearson's correlation coefficients varying from − 0.50 for capecitabine-treated tumors to + 0.42 for irradiated tumors.

Within 4 days of therapy, there were no statistically significant changes in mean tumor ADC (%ADC4) in the five treatment groups. However, a positive, but not significant, correlation between mean %ADC4 and mean ultimate tumor delay ($r = 0.77$, $P = .07$) was observed. There was a positive correlation between mean %ADC11 and mean tumor delay for the treatment groups ($r = 0.92$, $P < .01$), indicating a linear relationship between an early increase in tumor ADC and the ultimate effectiveness of therapy (Figure 7).

HT29 xenografts treated with capecitabine/oxaliplatin showed the same quantitative increase in mean %ADC11 as capecitabine/irradiation–treated tumors despite the fact that capecitabine/oxaliplatin was less efficacious than capecitabine/irradiation, with Td values of 14.1 and 26.5 days, respectively.

Tumor Histology

Histologic examination of HE stains showed that both treated and control tumors had necrotic centers. The necrotic fraction ranged from 12% to 84%. One-way ANOVA revealed no statistical differences in necrotic fractions between the six treatment groups ($P = .81$).

Discussion

Response to chemotherapy and/or radiotherapy may vary between individual tumors, and some tumors even proliferate during preoperative chemoradiation, suggesting a potential benefit if therapy response parameters could be predicted either before onset of therapy or early on during treatment. Such means of prediction and early monitoring would leave clinicians with the possibility of adjustments during the course of therapy, thus individualizing therapeutic strategy, which could affect patient survival. In this study, diffusion MRI was found to be a possible and early surrogate marker of antitumor effect in mice bearing HT29 xenografts and treated

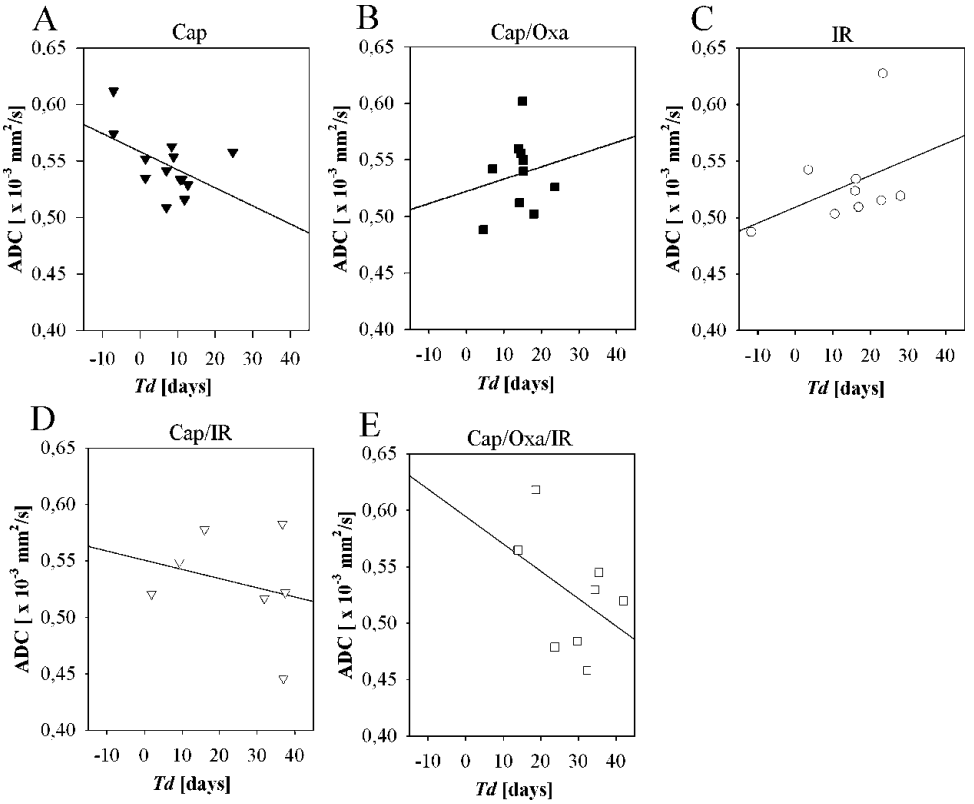

Figure 6. *Mean pretreatment tumor ADC as a function of tumor doubling growth delay (Td) for HT29 xenografts treated with (A) capecitabine, (B) capecitabine/oxaliplatin, (C) irradiation, (D) capecitabine/irradiation, and (E) capecitabine/oxaliplatin/irradiation. Solid lines represent linear regression fit lines.*

with a combination of the 5-FU prodrug capecitabine, oxaliplatin, and irradiation.

A treatment strategy with weekly oxaliplatin, daily capecitabine, and 2-Gy fractions of irradiation was chosen to mimic clinical situation. All treatments resulted in delayed tumor doubling time compared to the control group. Both oxaliplatin and capecitabine are potent radiosensitizing drugs [25–28] and, as expected, their radiosensitizing properties were observed in this study when chemotherapy was combined with irradiation, giving a significant increase in tumor doubling growth delay compared to the irradiated cohort. The combination of capecitabine and irradiation showed synergistic antiproliferative efficacy with an observed/expected tumor doubling growth delay ratio of 1.27. Capecitabine is

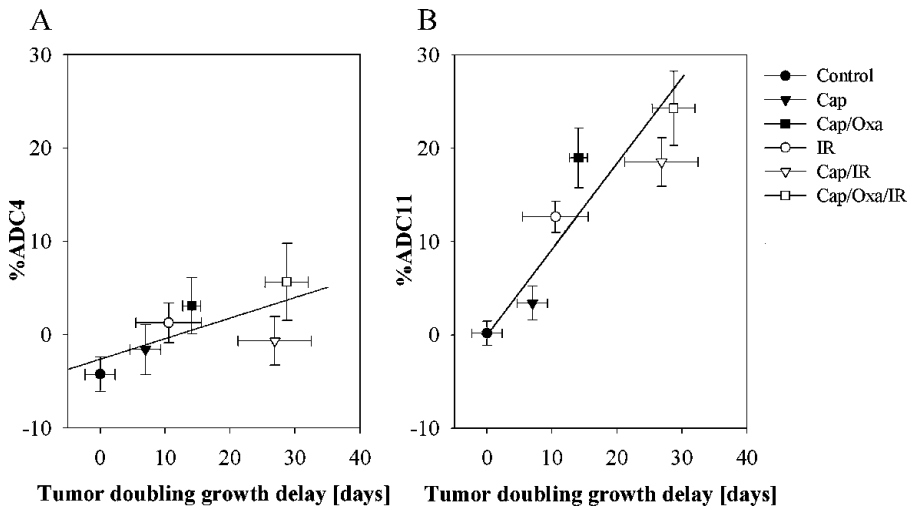

Figure 7. *Correlation between tumor doubling growth delay and ADC rise after 4 days (A) and 11 days (B) of therapy. ADC changes are given as percent changes compared to the pretreatment value. The six treatment groups are as follows: control (●), capecitabine (▼), capecitabine/oxaliplatin (■), irradiation (○), capecitabine/irradiation (▽), and capecitabine/oxaliplatin/irradiation (□). Error bars indicate SEM. Solid lines represent linear regression fit lines.*

converted to 5-FU in tumor cells by the enzyme thymidine phosphorylase, which is upregulated in tumor tissue compared to adjacent normal tissue [34], and the synergy between capecitabine and irradiation could be a result of irradiation-induced increase in tumor levels of thymidine phosphorylase expression in human xenografts [25]. The antitumor effect of capecitabine and irradiation was enhanced by adding oxaliplatin, indicating a potential for further improving antitumor efficacy for patients receiving preoperative chemoradiation by integrating oxaliplatin into the standard 5-FU–based chemotherapy strategy in rectal cancer.

By setting the tumor doubling time of the two xenografts (one in group 5 and one in group 6) that did not double their volumes to the maximum observation period (60 days), the antitumor effects in these two treatment groups are underestimated. Removal of these xenografts from the growth curves would have further underestimated the effect of these two therapeutic regimes. However, to avoid introducing errors in the evaluation of changes in ADC as an early measure of therapeutic efficiency, data from these two xenografts were excluded from these analyses.

DW-MRI provides information about microscopic structures such as cell density and integrity or necrosis. Thus, a viable tumor can be differentiated from a necrotic tumor with diffusion imaging in contrast to conventional MRI. Cell density and necrotic fractions are parameters that have been monitored with diffusion MRI [35–38]. A tissue with high cellular density shows a low ADC resulting from impeded mobility of water protons by a higher amount of cell membranes, whereas necrotic areas will appear as hyperintense areas on ADC maps resulting from the rapid diffusion of water protons as a consequence of lost membrane integrity [35,36]. Figure 8 shows the T_2-weighted MR images and ADC maps of two HT29 xenografts with 20% and 80% necrotic fractions. In most cases, the MR images showed some degree of heterogeneity due to localized necrotic regions with high water mobility/high signal on both T_2-weighted images and ADC maps. When using diffusion MRI for examining biologic effects, usually only the tumor periphery of viable cells is of interest, and successful separation between viable and necrotic areas relies on the skills of the operator. The entire tumor is easily delineated in T_2-weighted images. Information gathered from consideration of the entire tumor is readily applicable to the clinical evaluation of treatment outcome. Furthermore, failure to evaluate the entire tumor volume might result in sampling errors related to tumor heterogeneity (errors that are similar to those associated with invasive methods) because the sampled region may not be representative of the entire tumor [38].

A potential shortcoming in this study is the use of a single *b* value of 300 sec/mm^2. We did not investigate the role of different *b* values because a pilot study showed satisfactory results with a *b* value of 300 sec/mm^2 and because higher *b* values are associated with greater reduction in signal and lower image quality. But, as a quantitative parameter of DW-MRI, ADC reflects not only diffusion but also perfusion of microvessels [39]. Previous studies have shown that for low *b* values (b < 100 sec/mm^2), perfusion dominates diffusion by a factor of 10 [39,40]. By using high *b* values, the influence of perfusion is largely cancelled, and most of the signal remaining in the image originates from molecules with the lowest mobility, and the ADC value approximates true diffusion. The use of low and high *b* values in the same setting for the calculation of ADC could have provided more specific information about underlying biologic mechanisms.

Echo-planar imaging sequences will give diffusion images with good signal-to-noise ratio and low radiofrequency (RF) power deposition, but gradient rephasing results in spatial distortions from magnetic susceptibility effects, especially near air interfaces [14]. This will give rise to anatomic mismatch on coregistration with T_2-weighted MR images. RF-refocused single-shot fast spin-echo–based diffusion MR acquisitions provide images without a significant degree of spatial distortions.

In this study, we found no correlation between pretreatment tumor ADC values and regrowth delay for individual

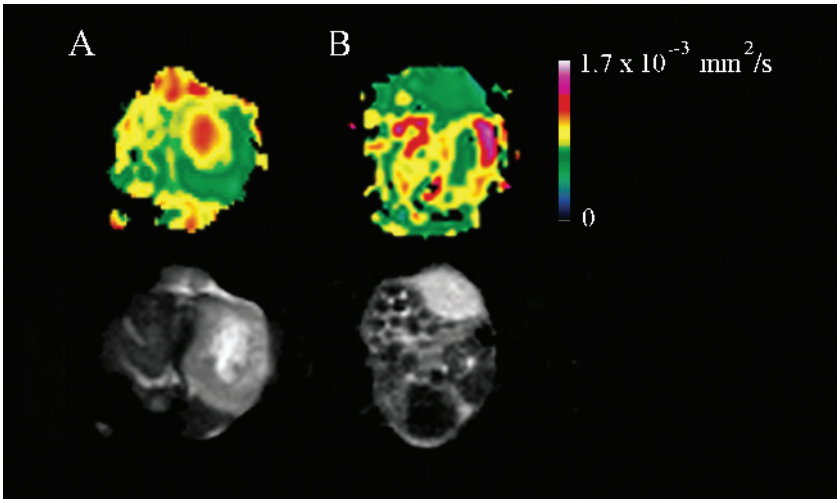

Figure 8. *ADC maps (upper row) and T_2-weighted images (bottom row) illustrating the differences between a tumor with a large necrotic central area (A) and a tumor with mostly viable cells (B). Histologic analysis of corresponding tumor slices revealed necrotic fractions of 80% and 20%, respectively, in these two tumors.*

tumors (Figure 6). It is a prerequisite for comparing different chemotherapy regimens in animal models that initial xenografts be similar so that observed effects are therapy-induced effects and not effects originating from the initial composition of necrosis, fibrosis, and viable cells in tumors. To the authors' knowledge, there has been only one published clinical study that shows a strong negative correlation between pretreatment ADCs and response to therapy for rectal carcinomas treated with chemoradiation [41]. In this study, mean pretreatment ADC values ranged from 0.8×10^{-3} to 2.2×10^{-3} mm^2/sec, indicating large differences in the initial composition of individual tumors and, hence, also sensitivity to therapy compared to xenografts in our experiment (0.4×10^{-3} to 0.6×10^{-3} mm^2/sec). Necrotic tumors have high ADC values and are also known to be associated with poor response to cancer treatment [41].

The therapeutic interventions in this study resulted in increased water mobility in the tumors observed as a rise in the mean tumor ADC, and 11 days after initialization, this increase was significant for all treatment tumors except for those receiving capecitabine only ($P = .06$). The increase in tumor water diffusion is consistent with results from other experimental tumors on treatment with other anticancer drugs and gene therapy [7–13,42–45]. The underlying mechanisms of changes in diffusion in tumors are not fully understood, but MR data from different tumor types tend to suggest that the density of viable cells might be the key factor affecting water diffusion in tumors [7,35]. As a response to therapy, tumor cells die and the membrane starts to degrade; therefore, extracellullar water fraction increases and gives an increased ADC value. It is tempting to extrapolate that the therapy-induced increase in ADC values is due to cell shrinkage, although the exact mechanism has not yet been determined.

In our study, the increase in tumor ADC measured 11 days after the onset of therapy (%ADC11) correlated with ultimate tumor response, and the magnitude of change was directly related to the effectiveness of the therapy. These results show that diffusion imaging has the potential for the early assessment of therapy response in individual patients. Because many treatment regimes such as chemotherapy and radiotherapy are frequently given in fractionated cycles, an early assessment of therapeutic response during the initial phase of administration would provide an opportunity to gauge optimum dosage and would also provide feedback related to optimum dose frequency. The sensitivity of diffusion MRI to changes in tissue structure may also advance experimental therapeutics by providing new tools for analyzing therapeutics both in laboratory models and in clinical work.

Despite large differences in tumor doubling growth delay between capecitabine/irradiation–treated and capecitabine/oxaliplatin–treated xenografts, their %ADC11 values were similar. This might be an indication of the quantitative amount of ruptured cell membranes (lysis) being equal in the two groups. Exposure to radiation has been shown to induce cellular senescence in some tumor cell lines [46]. Radiation-induced senescence would contribute to the growth delay of tumors without necessarily influencing the ADC. However, it is not known if radiation-induced senescence occurs in the HT29 xenografts used in this study, but the existence of such a mechanism in the capecitabine/irradiation group could explain the reduced tumor growth in these xenografts compared to that in the capecitabine/oxaliplatin group.

The full prognostic value of diffusion MRI remains unclear, and further work is required to determine whether the observed changes in tumor diffusion are a universal response to successful cell killing and to delineate the kinetics of diffusion changes, but our results suggest that early changes in ADC could yield clinically important information in the prediction of therapy response for rectal cancer.

Acknowledgement

The authors thank Marita Martinsen (Department of Tumor Biology, Rikshospitalet-Radiumhospitalet Medical Center) for excellent technical assistance.

References

[1] Parkin DM, Bray F, Ferlay J, and Pisani P (2001). Estimating the world cancer burden. Globocan. *Int J Cancer* **94**, 153–156.

[2] Heald RJ, Husband EM, and Ryall RDH (1982). The mesorectum in rectum cancer surgery: the clue to pelvic recurrence. *Br J Surg* **69**, 613–616.

[3] Glimelius B, Grönberg H, Järhult J, Wallgren A, and Cavallin-Ståhl E (2003). A systematic overview of radiation therapy effects in rectal cancer. *Acta Oncol* **42**, 476–492.

[4] Sauer R, Becker H, Hohenberger W, Rödel C, Wittekind C, Fietkau R, Martus P, Tschmelitsch J, Hager E, Hess CF, et al. (2004). Preoperative *versus* postoperative chemoradiotherapy for rectal cancer. *N Engl J Med* **351**, 1731–1740.

[5] Kim HK, Jessup JM, Beard CJ, Bornstein B, Cady B, Stone MD, Bleday R, Bothe A Jr, Steele G Jr, and Busse PM (1997). Locally advanced rectal carcinoma: pelvic control and morbidity following preoperative radiation therapy, resection, and intraoperative radiation therapy. *Int J Radiat Oncol Biol Phys* **38**, 777–783.

[6] Kapiteijn E, Marijnen CAM, Nagtegaal ID, Putter H, Steup WH, Wiggers T, Rutten HJ, Pahlman L, Glimelius B, van Krieken JH, et al. (2001). Preoperative radiotherapy combined with total mesorectal excision for resectable rectal cancer. *N Engl J Med* **345**, 638–646.

[7] Zhao M, Pipe JG, Bonnett J, and Evelhoch JL (1996). Early detection of treatment response by diffusion-weighted ^{1}H-NMR spectroscopy in a murine tumour *in vivo*. *Br J Cancer* **73**, 61–64.

[8] Moffat BA, Hall DE, Stojanovska J, McConville PJ, Moody JB, Chenevert TL, Rehemtulla A, and Ross BD (2004). Diffusion imaging for evaluation of tumor therapies in preclinical animal models. *MAGMA* **17**, 249–259.

[9] Kauppinen RA (2002). Monitoring cytotoxic tumour treatment response by diffusion magnetic resonance and proton spectroscopy. *NMR Biomed* **15**, 6–17.

[10] Evelhoch JL, Gillies RJ, Karczmar GS, Koutcher JA, Maxwell RJ, Nalcioglu O, Raghunand N, Ronen SM, Ross BD, and Swartz HM (2000). Applications of magnetic resonance in model systems: cancer therapeutics. *Neoplasia* **2**, 152–165.

[11] Ross BD, Moffat BA, Lawrence TS, Mukherji SK, Gebarski SS, Quint DJ, Johnson TD, Junck L, Robertson PL, Muraszko KM, et al. (2003). Evaluation of cancer therapy using diffusion magnetic resonance imaging. *Mol Cancer Ther* **2**, 581–587.

[12] Thoeny HC, De Keyzer F, Chen F, Vandecaveye V, Verbeken EK, Ahmed B, Sun X, Ni Y, Bosmans H, Hermans R, et al. (2005). Diffusion-weighted magnetic resonance imaging allows non-invasive *in vivo* monitoring of the effects of combretastatin A-4 phosphate after repeated administration. *Neoplasia* **7**, 779–787.

[13] Moffat BA, Chenevert TL, Meyer CR, Mckeever PE, Hall DE, Hoff BA, Johnsom TD, Rehemtulla A, and Ross BD (2006). The functional diffusion map: an imaging biomarker for the early prediction of cancer treatment outcome. *Neoplasia* **8**, 259–267.

[14] Vlaardingerbroek MT and den Boer JA (1999). Magnetic Resonance Imaging, 2nd ed, Springer, New York, pp. 354–360.
[15] Jordan BF, Runquist M, Raghunand N, Baker A, Williams R, Kirkpatrick L, Powis G, and Gillies RJ (2005). Dynamic contrast-enhanced and diffusion MRI show rapid and dramatic changes in tumor microenvironment in response to inhibition of HIF-1α using PX-478. *Neoplasia* **7**, 475–485.
[16] Malet-Martino M and Martino R (2002). Clinical studies of three oral prodrugs of 5-fluorouracil (capecitabine, UFT, S-1): a review. *Oncologist* **7**, 288–323.
[17] Glynne-Jones R, Dunst J, and Sebag-Montefiore D (2005). The integration of oral capecitabine into chemoradiation regimens for locally advanced rectal cancer: how successful have we been? *Ann Oncol* **17**, 361–371.
[18] Calvo FA, Serrano FJ, Diaz-González JA, Gomez-Espi M, Lozano E, Garcia R, de la Mata D, Arranz JA, Garciá-Alfonso P, Pérez-Manga G, et al. (2006). Improved incidence of pT_0 downstaged surgical specimens in locally advanced rectal cancer (LARC) treated with induction oxaliplatin plus 5-fluorouracil and preoperative chemoradiation. *Ann Oncol* **17**, 1103–1110.
[19] Machiels J-P, Duck L, Honhon B, Coster B, Coche J-C, Scalliet P, Humblet Y, Aydin S, Kerger J, Remouchamps V, et al. (2005). Phase II study of preoperative oxaliplatin, capecitabine and external beam radiotherapy in patients with rectal cancer: the RadiOxCape Study. *Ann Oncol* **16**, 1898–1905.
[20] Zeuli M, Nardoni C, Pino MS, Gamucci T, Gabriele A, Ferraresi V, Giannarelli D, and Cognetti F (2003). Phase II study of capecitabine and oxaliplatin as first-line treatment in advanced colorectal cancer. *Ann Oncol* **14**, 1378–1382.
[21] Aschele C, Friso ML, Pucciarelli S, Lonardi S, Sartor L, Fabris G, Urso EDL, Del Bianco P, Sotti G, Lise G, et al. (2005). A phase I–II study of weekly oxaliplatin, 5-fluorouracil continuous infusion and preoperative radiotherapy in locally advanced rectal cancer. *Ann Oncol* **16**, 1140–1146.
[22] Rutten H, Sebag-Montefiore D, Glynne-Jones R, Rullier E, Peeters M, Brown G, Van Cutsem E, Ricci S, Van de Velde CJ, and Quirke P (2006). Capecitabine, oxaliplatin, radiotherapy, and excision (CORE) in patients with MRI-defined locally advanced rectal adenocarcinoma: results of an international multicenter phase II study. *J Clin Oncol (Meet Abstr)* **24**, 3528.
[23] Gerard JP, Chapet O, Nemoz C, Romestaing P, Mornex F, Coquard R, Barbet N, Atlan D, Adeleine P, and Gilles F (2003). Preoperative concurrent chemoradiotherapy in locally advanced rectal cancer with high-dose radiation and oxaliplatin-containing regimen: the Lyon R0-04 phase II trial. *J Clin Oncol* **21**, 1119–1124.
[24] Minsky BD (2003). Oxaliplatin-based combined-modality therapy for rectal cancer. *Semin Oncol* **30**, 26–33.
[25] Sawada N, Ishikawa T, Sekiguchi F, Tanaka Y, and Ishitsuka H (1999). X-ray irradiation induces thymidine phosphorylase and enhances the efficacy of capecitabine (Xeloda) in human cancer xenografts. *Clin Cancer Res* **5**, 2948–2953.
[26] Magne N, Fischel JL, Formento P, Erienne MC, Dubreuil A, Marcie S, Lagrange JL, and Milano G (2003). Oxaliplatin–5-fluorouracil and ionizing radiation. Importance of the sequence and influence of p53 status. *Oncology* **64**, 280–287.
[27] Kjellstrom J, Kjellen E, and Johansson A (2005). *In vitro* radiosensitization by oxaliplatin and 5-fluorouracil in a human colon cancer cell line. *Acta Oncol* **44**, 687–693.
[28] Cividalli A, Ceciarelli F, Lividi E, Altavista P, Cruciani G, Marchetti P, and Danesi DT (2002). Radiosensitization by oxaliplatin in a mouse adenocarcinoma: influence of treatment schedule. *Int J Radiat Oncol Biol Phys* **52**, 1092–1098.
[29] Rödel C, Grabenbauer GG, Papadopoulos T, Hohenberger W, Schmoll HJ, and Sauer R (2003). Phase I/II trial of capecitabine, oxaliplatin, and radiation for rectal cancer. *J Clin Oncol* **21**, 3098–3104.
[30] Glynne-Jones R, Sebag-Montefiore D, Maughan TS, Falk SJ, and McDonald AC (2006). A phase I dose escalation study of continuous oral capecitabine in combination with oxaliplatin and pelvic radiation (XELOX-RT) in patients with locally advanced rectal cancer. *Ann Oncol* **17**, 50–56.
[31] Machiels JPP, Duck L, Honhon B, Coster B, Coche JP, Scalliet P, Humblet Y, Aydin S, Kerger J, Remouchamps V, et al. (2005). Phase II study of preoperative oxaliplatin, capecitabine, and external beam radiotherapy in patients with locally advanced rectal adenocarcinoma: the RadiOxCape Study. *Ann Oncol* **16**, 1898–1905.
[32] Fakih MG, Rajput A, Yang GY, Pendyala L, Toth K, Smith JL, Lawrence DD, and Rustum YM (2006). A Phase I study of weekly intravenous oxaliplatin in combination with oral daily capecitabine and radiation therapy in the neoadjuvant treatment of rectal adenocarcinoma. *Int J Radiat Oncol Biol Phys* **1**, 1462–1470.
[33] Balin-Gauthier D, Delord JP, Rochaix P, Mallard V, Thomas F, Hennebelle I, Bugat R, Canal P, and Allal C (2006). *In vivo* and *in vitro* antitumor activity of oxaliplatin in combination with cetuximab in human colorectal tumor cell lines expressing different level of EGFR. *Cancer Chemother Pharmacol* **57**, 709–718.
[34] Miwa M, Ura M, Nishida M, Sawada N, Ishikawa T, Mori K, Shimma N, Umeda I, and Ishitsuka H (1998). Design of a novel oral fluoropyrimidine carbamate, capecitabine, which generates 5-fluorouracil selectively in tumours by enzymes concentrated in human liver and cancer tissue. *Eur J Cancer* **34**, 1274–1281.
[35] Lyng H, Haraldset O, and Rofstad EK (2000). Measurement of cell density and necrotic fraction in human melanoma xenografts by diffusion weighted magnetic resonance imaging. *Magn Res Med* **43**, 828–836.
[36] Herneth AM, Guccione S, and Bednarski M (2003). Apparent diffusion coefficient: a quantitative parameter for *in vivo* tumor characterization. *Eur J Radiol* **45**, 208–213.
[37] Evelhoch JL (1999). Key factors in the acquisition of contrast kinetic data for oncology. *J Magn Reson Imaging* **10**, 254–259.
[38] Gillies RJ, Bhujwalla ZM, Evelhoch J, Garwood M, Neeman M, Robinson SP, Sotak CH, and Van Der Sanden B (2000). Applications of magnetic resonance in model systems: tumor biology and physiology. *Neoplasia* **2** (1–2), 139–151.
[39] Le Bihan D, Breton E, Lallemand D, Aubin ML, Vignaud J, and Laval-Jeantet M (1988). Separation of diffusion and perfusion in intravoxel incoherent motion MR imaging. *Radiology* **168**, 497–505.
[40] Morvan D (1995). *In vivo* measurement of diffusion and pseudo-diffusion in skeletal muscle at rest and after exercise. *Magn Reson Imaging* **13**, 193–199.
[41] Dzik-Jurasz A, Domenig C, George M, Wolber J, Padhani A, Brown G, and Doran S (2002). Diffusion MRI for prediction of response of rectal cancer to chemoradiation. *Lancet* **360**, 307–308.
[42] Chenevert TL, Stegman LD, Taylor JM, Robertson PL, Greenberg HS, Rehemtulla A, and Ross BD (2000). Diffusion magnetic resonance imaging: an early surrogate marker of therapeutic efficacy in brain tumors. *J Natl Cancer Inst* **92**, 2029–2036.
[43] Galons JP, Altbach MI, Paine-Murrieta G, Taylor CW, and Gilles RJ (1999). Early increases in breast tumor xenografts water mobility in response to paclitaxel therapy detected by non-invasive diffusion magnetic resonance imaging. *Neoplasia* **1**, 113–117.
[44] Poptani H, Puumalainen A-M, Gröhn OHJ, Loimas S, Kainulainen R, Ylä-Herttuala S, and Kauppinen RA (1998). Monitoring thymidine kinase and ganciclovir-induced changes in rat malignant glioma *in vivo* by nuclear magnetic resonance imaging. *Cancer Gene Ther* **5**, 101–109.
[45] Theilmann RJ, Borders R, Trouard TP, Xia G, Outwater E, Ranger-Moore J, Gillies RJ, and Stopeck A (2004). Changes in water mobility measured by diffusion MRI predict response of metastatic breast cancer to chemotherapy. *Neoplasia* **6**, 831–837.
[46] Zhou B-BS and Bartek J (2004). Targeting the checkpoint kinases: chemosensitization *versus* chemoprotection. *Nat Rev Cancer* **4**, 1–10.